RADIO SCIENCE, VOL. 48, 1-9, doi:10.1029/2012RS005034, 2013

On the characterization of radar receivers for meteor-head echoes studies

F. R. Galindo,[1] J. Urbina,[1] J. L. Chau,[2] L. Dyrud,[3] and M. Milla[2]

Received 30 March 2012; revised 7 November 2012; accepted 27 November 2012.

[1] We report the role that the ambiguity function (AF) plays on the determination of signal to noise ratio (SNR) collected from meteor head echoes. Theoretical analysis shows that any measured meteor SNR exhibits temporal ripples whose shape is related to both the transmitted pulse envelope and the filter impulse response of the receiver. These theoretical findings are corroborated with (1) experimental meteor data recorded with Jicamarca 50 MHz radar (11.95° S, 76.87° W) and (2) simulated meteor data obtained by replicating the acquisition system of Jicamarca. A statistical analysis of the experimental meteor data reveals that at least 14% of the population collected each day at Jicamarca exhibits these ripples. On the remaining 86% of meteor events, the ripples cannot be distinguished due to noise, contamination from other sources of scattering (i.e., nonspecular echoes), and ensemble average applied to the data. In general, these ripples demonstrate the importance of obtaining an accurate model of a radar system to avoid misinterpretation of SNR.

Citation: Galindo, F., J. Urbina, J. L. Chau, L. Dyrud, and M. Milla (2013), On the characterization of radar receivers for meteor-head echoes studies, *Radio Sci.*, *48*, doi: 10.1029/2012RS005034.

1. Introduction

[2] Since the mid 1990s, High Power-Large Aperture (HPLA) radars such as ALTAIR, Arecibo, EISCAT, and Jicamarca have proven to be excellent tools for conducting meteor research. HPLA radars can detect scatter from the plasma spheres which surround ablating meteoroids. This scatter data can be used to infer meteoroid parameters such as mass, speed, and other properties. For example, *Chau and Woodman* [2004] used Jicamarca 50 MHz radar to show that the detected meteors were concentrated around theEarth's Apex, and *Chau and Galindo* [2008] proved that HPLA radars can observe meteor shower populations. More recently, *Mathews et al.* [2010] reported meteor observations collected with the VHF and UHF Arecibo radars that seemed consistent with meteoroid fragmentation, and *Vertatschitsch et al.* [2011] presented results from a numerical electromagnetic model of fragmentation. These recent investigations show considerable progress in meteor physics using HPLA radars; however, very few studies have been conducted to fully characterize current radar systems in order to correctly infer meteor parameters. One example is the work by *Chau et al.* [2009] which characterized the impact of the antenna beam pattern on the received power of meteor head echoes. Their results indicated that at least 15% of the meteors observed with the 450 MHz Poker Flat incoherent scatter radar were detected from the sidelobes of the antenna. Therefore the power of these meteors had to be corrected by about ~20 dB to be considered that these events were coming from the main beam of the antenna. These corrections are needed in order to apply current techniques to extract meteor information from the received power [*Close et al.*, 2004; *Janches et al.*, 2009].

[3] In this paper we assess the role that the ambiguity function plays on the characterization of SNR from meteor head echoes. This analysis is presented by expressing the radar equation for meteor head echoes in terms of the ambiguity function (AF) [*Woodman*, 1991; *Milla and Kudeki*, 2006] of the transmitted pulse envelope and the filter impulse response of the radar receiver. Our results show that any meteor SNR, i.e., SNR collected from a meteor head echo, exhibit temporal ripples to various degrees. These ripples illustrate the importance of obtaining an accurate model of a radar system in order to correctly estimate meteor SNR and subsequently infer other meteor parameters from the SNR. Our theoretical findings are verified by using experimental data collected with the Jicamarca radar and simulated data obtained by replicating the acquisition system of Jicamarca. Additionally, a statistical study on actual meteor data reveals that at least 14% of the population collected each day at Jicamarca exhibit these ripples. On the remaining 86% of events, the ripples cannot be distinguished due to noise, contamination from other sources of scattering (i.e., nonspecular echoes), and ensemble average applied to the data. Therefore any approach such as inversion techniques to infer unbiased meteor parameters must account for the effect of these temporal ripples.

[1]Communications and Space Sciences Laboratory, Department of Electrical Engineering, The Pennsylvania State University, University Park, Pennsylvania, 16802, USA.
[2]Radio Observatorio de Jicamarca, Instituto Geofisico del Peru, Lima, Peru.
[3]Johns Hopkins University, Applied Physics Laboratory, Baltimore, Maryland, USA.

Corresponding author: F. Galindo, Communications and Space Sciences Laboratory, Department of Electrical Engineering, The Pennsylvania State University, University Park, Pennsylvania 16802, USA. (frg5014@psu.edu)

0048-6604/13/2012RS005034

[4] Our paper is organized as follows: Section 2 describes the radar equation for meteor head echoes and presents the AF for Jicamarca HPLA radar receiver. Section 3 shows two meteor head echoes detected with Jicamarca and describes the features observed in their SNR by using the AF analysis. In addition, we present a statistical study of 3 days of meteor observations conducted at Jicamarca, where we show that at least 14% of actual meteor data exhibit the temporal ripples analyzed in this paper. In section 4, we present a simulator of the Jicamarca radar receiver. In section 5, we discuss the role of radar parameters that affect the shape and amplitude of the ripples. Finally, we provide a summary of this research in section 6.

2. Characterization of Radar Receivers

[5] In this section, we derive the radar equation for meteor head echoes and apply this equation to a meteor experiment by using Jicamarca radar. Furthermore, we demonstrate the importance of the ambiguity function in the determination of meteor SNR.

2.1. Meteor Head Radar Equation

[6] The radar equation for meteor head echoes can be constructed by considering meteor head echoes as point scatterers [*Close et al.*, 2002; *Roy et al.*, 2009] and by using a simplified monostatic radar configuration as shown in Figure 1. In Figure 1 the transmitter and receiver are separated to illustrate the general process of radar observation. On transmission, the carrier signal w_0 is modulated with the transmitted pulse envelope *f(t)* and sent to space. A signal is scattered back to the receiving antenna when a meteor is present at a distance *r(t)* from the antenna of transmission, as depicted in Figure 1. The received signal collected at the input of terminals is then converted to baseband to produce the received voltage $v_p(t)$. This voltage $v_p(t)$ is then convolved with the impulse response *h(t)* of the receiver filter to produce the measured voltage *v(t)*. This operation can be denoted as

$$v(t) = v_p(t) * h(t) = \int v_p\left(\tau'\right)\ h\left(t-\tau'\right)d\tau' \tag{1}$$

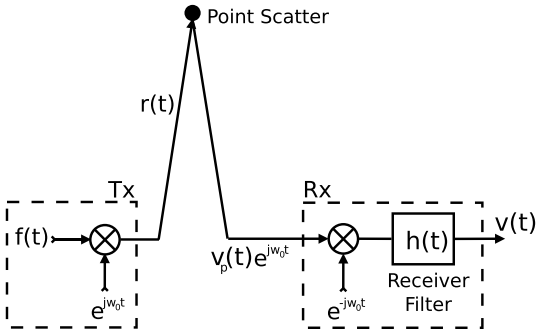

Figure 1. Simplified monostatic radar configuration for a meteor head echo. The received voltage $v_p(t)e^{jw_0t}$ is transformed to base band and then convolved with the receiver filter. The voltage *v(t)* represents the actual measurement. Note that we have separated the transmission and receiver to clearly illustrate the process.

[7] Suppose the meteor head echo is traveling at constant Doppler velocity v_r; then it is possible to express its variable range as

$$r(t) = r_0 + v_r t \tag{2}$$

where r_0 denotes the initial detection range of the meteor and t represents time. Subsequently, the received voltage $v_p(t)$ can be expressed as follows [*Kudeki*, 2006]:

$$v_p(t) = Z(r(t))f\left(t-\frac{2r(t)}{c}\right)e^{-j2k_0r_0-j\frac{4\pi}{\lambda}v_rt} \tag{3}$$

where $|Z(r(t))|^2 = 4I_0^2R_{rad}^2\left[GA/(4\pi r^2(t))^2\right]\sigma_p$, σ_p is the radar cross section (RCS) of the target; I_0 and R_{rad} are the current and resistance of antenna of transmission, respectively; xtitG is the antenna gain in the direction of the target; A is the effective area of the antenna; k_0 is the radar wavenumber; λ is the radar wavelength; and c is the speed of light. Replacing equation (3) in equation (1), the measured voltage *v(t)* can be written as

$$v(t) = \int Z\left(r(\tau')\right)f\left(\tau' - \frac{2r(\tau')}{c}\right)h\ \left(t-\tau'\right)e^{-j2k_0r_0-j\frac{4\pi}{\lambda}v_r\tau'}d\tau' \tag{4}$$

and therefore the measured power P_r is

$$P_r = \frac{1}{2}I_0R_{rad}\frac{GA}{4\pi r_0^2}\sigma_p\frac{1}{4\pi r_0^2}\left|\int f\left(\tau'\right)h\left(\left(t-\frac{2r(\tau')}{c}\right)-\tau'\right)\right. \left.e^{-j\frac{4\pi}{\lambda}v_r\tau'}d\tau'\right|^2 \tag{5}$$

[8] Equation (5) has been deduced assuming that changes in range due to the meteor movement are smaller than the range resolution of the radar pulse, i.e., $r(t) \approx r_0$.

[9] Next, suppose the thermal noise N_r [*Nyquist*, 1928] in the radar receiver can be approximated by

$$N_r = kT_sB \tag{6}$$

where k represents the Boltzmann constant, T_s is the system noise temperature, and B is the receiver bandwidth. Thus the measured SNR can be expressed as

$$SNR = \frac{1}{2}\frac{1}{kT_sB}I_0^2R_{rad}\frac{GA}{4\pi r_0^2}\sigma_p\frac{1}{4\pi r_0^2}\left|\int f\left(\tau'\right)h\left((t-\frac{2r(\tau')}{c})-\tau'\right)\right. \left.e^{-j\frac{4\pi}{\lambda}v_r\tau'}d\tau'\right| \tag{7}$$

[10] Equation (7) shows that the received SNR is modulated by a nondimensional system function that takes into account the effects of the transmitted pulse envelope *f(t)* and receiver filter impulse response *h(t)*. This system function is called the ambiguity function of the radar receiver and is defined [*Siebert*, 1956; *Levanon*, 1988] as

$$\chi(\tau, v_r) = \int f\left(\tau'\right)\ h\left(\tau-\tau'\right)e^{-j\frac{4\pi}{\lambda}v_r\tau'}d\tau' \tag{8}$$

where τ is the delay with respect to the initial reference time, i.e., initial detection range. Equation (8) demonstrates that

the SNR is affected by the position of the meteor and its Doppler velocity. In the following subsection, we show thatmeteor SNR inevitably exhibits ripples due to the position of the meteor within a range cell. These ripples are only a function of the delay in range.

2.2. Implementation of the Ambiguity Function

[11] The results of equation (8) are applied to a typical meteor experiment with the Jicamarca radar [*Chau et al*, 2007]. This type of configuration uses a pulse width of 13 μs (i.e., 1950 m), a 13 baud Barker phase code for transmission, and an effective sampling rate equal to 1 MHz (i.e. 150 m) for reception. The effective sampling rate is accomplished by using an analog to digital converter at a high-speed rate of 60 MHz and a digital down-conversion (DDC) stage (see Figure 2). The outputof the DDC is the amplitude and phase information of meteor head echo, decimated down to the required sampling rate, i.e., effective sampling rate. Details about the down converter and filter coefficients can be found in the GC 4016 Multi-Standard Quad DDC Chip-Data Sheet, 2001.

[12] In this study, the AF is calculated by considering a pulse length equal to 1 μs (i.e., 150 m) for the transmitted pulse envelope. This short pulse is analyzed to describe the characteristics of the AF, but our results are also valid for coded pulses since coded pulses are equivalent to short pulses after the decoding process is completed. We also considered the receiver filter impulse response equal to the total receiver filter impulse response of the radar receiver. This value is therefore the convolution of the CIC, CFIR, and PFIR filters (see Figure 2). Notice, we assumed that the coarse gain and the resampler stages do not introduce biases in the received signal. Figure 3a depicts a contour plot of the corresponding $|\chi(\tau,v_r)|$ while Figure 3b shows a profile cut of $|\chi(\tau,v_r)|$ along a constant Doppler velocity of ~70.81 km/s. These plots were generated using a sampling rate of 60 MHz in order to reproduce the speed of the analog to digital converter used at Jicamarca. In Figure 3b these samples are represented as blue diamonds. Furthermore, Figure 3b depicts the final output of the receiver due to the effective sampling of the system, shown as red circle. The region between the dashed lines shown in Figure 3b represents the corresponding radar range resolution. We plotted this egion to emphasize that the ripples in SNR values are produced due to changes in the range of meteor head echoes inside the range resolution. From Figures 3a and 3b we can determine the following features of the AF:

1. The Doppler velocity of meteor head echoes, i.e., from 10 to 72 km/s, does not show a noticeable effect on the profile cut of $|\chi(\tau,v_r)|$. Therefore the value of $|\chi(\tau,v_r)|$ is only a function of the delay in range, i.e., Figure3b is applicable for any Doppler velocity.

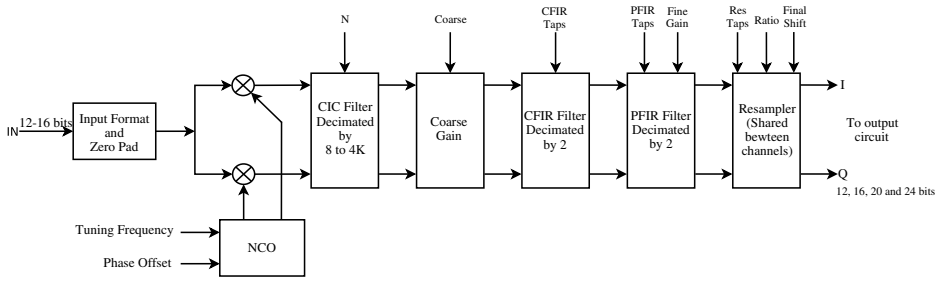

Figure 2. Block diagram of the digital down-converter stage of the HPLA Jicamarca radar receiver.

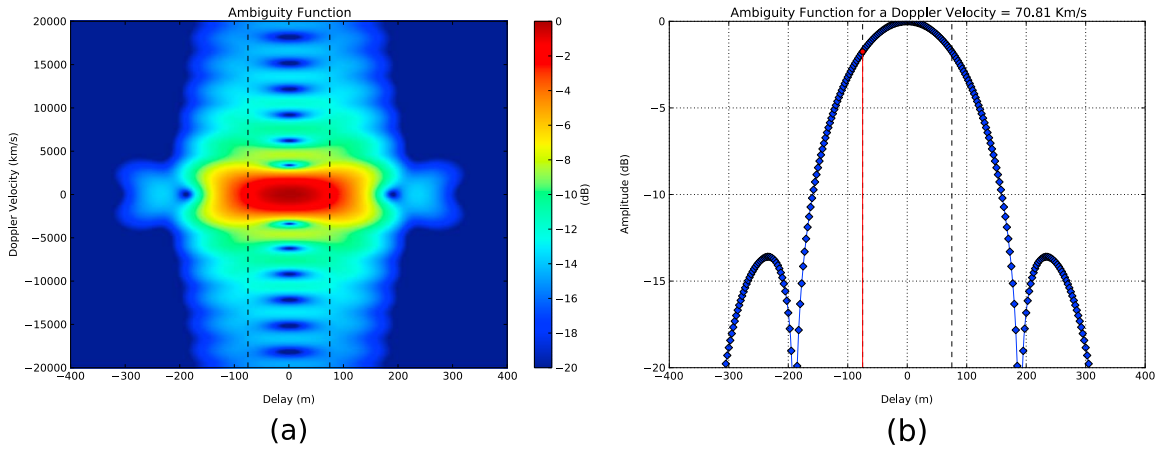

Figure 3. (a) Ambiguity function $|\boldsymbol{\chi(\tau,v_r)}|$ for a meteor observation at Jicamarca using a pulse with length T = 1 $\boldsymbol{\mu}$s. The receiver filter used for ambiguity function is the total response filter of the system. (b) A cut of the ambiguity function for a Doppler velocity ~70.81 km/s. The red line represents the actual data obtained after the decimation. The dashed lines in both plots represent the resolution. The horizontal axis in both plots represent the delay with respect to the initial range.

2. The effective sampling captures different values of $|\chi(\tau,v_r)|$ from -75 m to 75 m from consecutive radar pulse returns due to the fast-moving nature of the meteors.
3. During the effective sampling process, the maximum change in range is 150 m. Larger changes in range indicate that received power is coming from a different range bin.

[13] As a result of these characteristics, any meteor SNR will exhibit temporal ripples at any Doppler velocity but the detection of these ripples in actual meteor data depends on other sources of scattering, as well as signal processing performed on the data.

3. HPLA Meteor Observations

[14] This section complements the findings from section 2 with experimental observations and describes the features observed in SNR by using the ambiguity function. Furthermore, we present the outcome of statistical study of 3 days of meteor observations.

3.1. Signal to Noise Ratio

[15] We show in Figures 4a, 4b, and 4c, range-time intensity (RTI), range-time information, and SNR and Doppler velocity plots, respectively, for a meteor event detected on 27 February 2006 at Jicamarca. Notice that Figure 4a presents a longer time scale because it displays the entire meteor echo and its surroundings, while Figures 4b and 4c present the data selected for the processing. The range clutter observed in Figure 4a is associated to saturation of the Barker code sidelobes. The observation displayed in Figure 4 used the experimental parameters shown in Table 1, the typical meteor head configuration for the receiver system described in section 2 and an ensemble average of 4 interpulse period (IPP). The SNR, shown in Figure 4c, were determined as follows: (1) only the echo region of the meteor in range and time is selected from the RTI, (2) the corresponding peak SNR from each IPP is chosen and stored in an array, and (3) these peak SNR values were normalized with respect to the maximum SNR value of the array to emphasize the ripples and for this reason the SNR shows negative values. Details about the meteor head echo processing at Jicamarca can be found in *Chau and Woodman* [2004] and *Chau et al*. [2007]. Figure 4c shows two important features: (1) the overall modulation in the SNR was caused by the antenna pattern and (2) the small fluctuations in the SNR, which coincide very closely with the changes in range of the meteor head echo seen in Figure 4b. Figure 5 shows another example, but from an observation made on 5 May 2007. Table 1 also shows the corresponding experimental radar parameters for this observation.

[16] Herein, these small fluctuations are explained by using the AF presented in Figure 3b, an IPP = 0.4 ms, and a meteor head echo with constant Doppler velocity equal

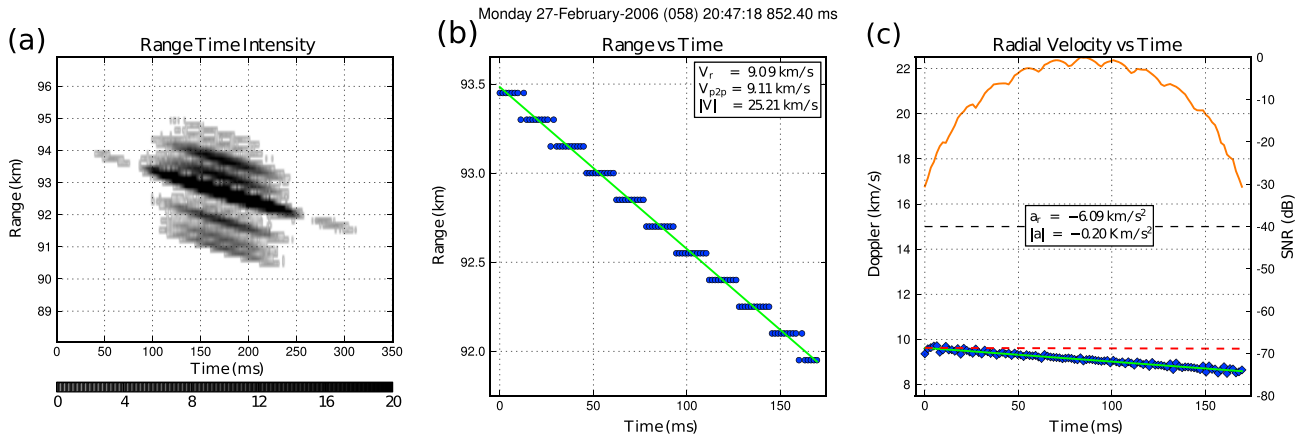

Figure 4. Meteor head event detected on 27 February 2006. (a) Range-time intensity map, (b) range versus time plot, and (c) pulse-to-pulse Doppler velocity estimates and normalized SNR plots. Figure 4a displays the meteor echo and its surroundings, while Figure 4b and 4c only display the data selected for the meteor processing.

Table 1. Experimental Parameters for the Three Meteor Head Observations at Jicamarca[a]

Parameters	February 2006	May 2007	December 2008
Interpulse period, km	60	60	129.6
Code	Barker-13	Barker-13	Barker-13
Baud width, km	0.15	0.15	0.30
Altitude coverage, km	85.05-123.5	85.05-123.5	85.05-133.05
Sampling, μs	1	1	2
Receiver type	digital	digital	digital
Duration, h	9	4	6
Population	1838	16885	14621
Meteors with SNR fluctuations, %	21.95	17.00	14.31

[a]The duration, total number of meteor events, and number of meteor events showing fluctuations are presented.

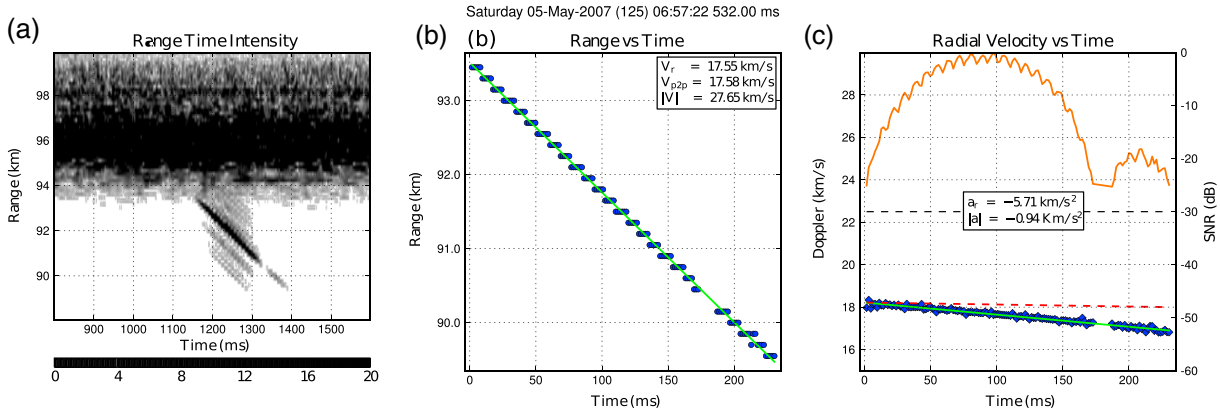

Figure 5. Similar to Figure 4, but showing an event from 5 May 2007.

to 12.5 km/s. This Doppler velocity is used to simplify the approach; however, the explanation can be extended to any Doppler velocity and therefore for the situations shown in Figures 4 and 5, which show Doppler velocities of ~9.09 km/s and ~17.55 km/s, respectively. This meteor head echo produces a change in range equal to ~5 m for every IPP during a meteor observation. If we consider that the initial range where the meteor is detected begins at a delay = -75 m as it is shown in Figure 3b, then during the subsequent IPPs, the effective sampling will collect values of $|\chi(\tau,v_r)|$ at delay = -70 m, -65 m, -60 m, and so on. As a result of this process, the effective sampling and therefore peak power detection will take different sections of $|\chi(\tau,v_r)|$ between -75 and 75 m. When the meteor head echo has traveled a distance of 150 m, i.e., the meteor is located at delay = 75 m, the receiver signal corresponds to the next range bin and therefore the changes in range are now measured with respect to this new range bin. Using this new range bin as an initial meteor range, we can repeat the process described lines above. In general, this process is repeated until the target is not present anymore within the radar view. Our previous consideration supports the assumption $r(t) \approx r_0$ made to derive equation (5) because the changes in range are measured with respect to the range bin. Therefore these changes in range are always smaller than the effective radar range resolution.

[17] The process previously explained demonstrates that meteor head echoes will present a step-like behavior in range-time diagrams, as it is shown in Figures 4b and 5b, because the effective sampling captures fixed positions in range. Furthermore, themeteor SNR will exhibit temporal ripples, as it is shown in Figures 4c and 5c, due to the effect of Doppler velocity of the meteor in displacing the AF in range. In other words, the SNR values will show ripples which are correlated with the changes in range, as observed in Figures 4b, 4c, 5b, and 5c. We should also note that the number of IPPs used to travel through the range resolution is inversely proportional to the Doppler velocity. In our case, the meteor head echo will need 30 IPPs approximately to travel 150 m. For higher Doppler velocities the changes in range will be longer and therefore fewer IPPs will be needed to travel through the range resolution. For example, for a Doppler velocity equal to 62.5 km/s, the number of IPPs is ~6. Therefore IPP value is an important parameter to discriminate the ripples after the signal processing is performed, i.e., ensemble average. The ripples showed in Figures 4c and 5c are produced by the same process previously described, but notice that the changes in range are different.

3.2. Statistical Analysis

[18] In previous sections, we showed that in general the temporal ripples could be observed in all detected meteors. However, in actual data, these ripples cannot be distinguished due to noise, other sources of scattering (e.g., nonspecular echoes), the signal processing performed in the data, and the radar configuration. In this section we present a statistical study to measure the actual value of events that show ripples in SNR. Our study selected 3 days of observations: 27 February 2006 from 15:00 to 24:00 LT, 5 May 2007 from 04:00 to 08:00 LT, and 14 December 2008 from 00:00 to 06:00 LT. Table 1 summarizes the experimental parameters of these days and the number of meteor head events showing ripples. Note that the three observations used a 13-bit Barker code and the radar receiver described in section 2.2. The IPP and effective sampling rate for 2008 were twice the value used in 2006 and 2007. Further, the observations from 2006 and 2007 used an ensemble average of 4 IPPs and the observation from 2008 only used two IPPs.

[19] The statistical summary of these meteor observations are shown in Table 1. This table indicates that at least 14% of the meteor events observed daily at Jicamarca presents temporal ripples in their SNR. Thus any approach (e.g., inversion techniques) used to correctly infer meteor parameters from SNR should account for these temporal effects on these events.

4. Radar Receiver Simulator

[20] In addition to the mathematical approach described in section 2, we constructed a simulator of the receiver system of Jicamarca radar to reproduce the main features observed in SNR plots. This simulator is a first-order approach that was built in two steps. The first step simulates the meteor head echo using the point target radar equation. Both amplitude and phase are computed for different instances of time using the radar equation. The multiple channels are obtained by changing the position of the antenna of reception. The amplitude from the radar equation was weighted using the theoretical antenna beam pattern model

of the Jicamarca antenna [*Ochs*, 1965] to allow comparison of simulated and experimental results. The data was simulated in baseband and an ideal sampling process at 60MHz was used. Moreover, the bandwidth effects of the antenna were not considered in the simulator. The second step simulates the down-conversion process (see Figure 2), where samples obtained at 60MHz are reduced to the final sampling rate. For our simulator we did not consider the baseband transformation, the coarse gain stage, and the resampler process. Despite these simplifications, the simulator agrees with the experimental observations. The final output of the complete simulator is the amplitude and phase information of meteor head echo.

[21] The simulator was evaluated assuming one target, using the meteor head configuration from 5 May 2007 (see Table 1) and no ensemble average. Figures 6 and 7 show meteor events with radial velocities equal to ~25 km/s and ~60 km/s, respectively. Figures 6 and 7 show the ripples observed in the experimental data as a result of sampling different sections of the AF. We observe that the shape of the temporal ripple does not depend on the radial velocity of the meteor and it corroborates that the value of $|\chi(\tau,v_r)|$ is only a function of the delay in range. We also observe that the number of IPPs related to the ripple is equivalent to the time the meteor event needs to travel through the radar range resolution (see Figures 6a and 7a).

[22] Figure 8 shows the meteor event presented in Figure 4 and the results produced by our simulator. In Figure 8 the range-time and velocity-time information for the simulated and experimental data are represented by blue and red color, respectively. In the case of the normalized SNR, we used green for the experimental data and orange for the simulator. The agreement between experimental and simulated data is clearly seen in Figure 8.

5. Discussions

[23] The results presented in previous sections demonstrate the importance of characterizing current radar system for meteor head studies to infer unbiased meteor parameters from SNR. This radar characterization implies that the information about the pulse envelope, the receiver filter,

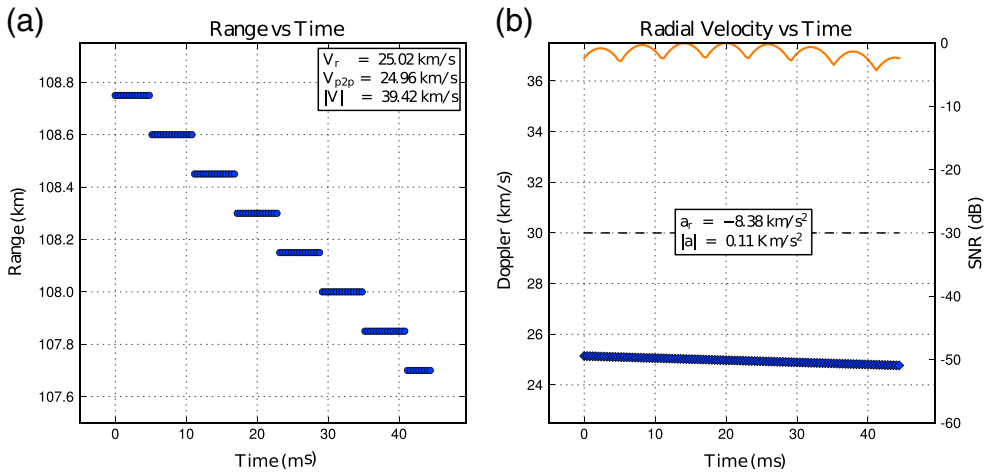

Figure 6. Simulated meteor head parameters for an event with ~25 km/s radial velocity. Note the correlation between both the ripples in the normalized SNR and the changes in range.

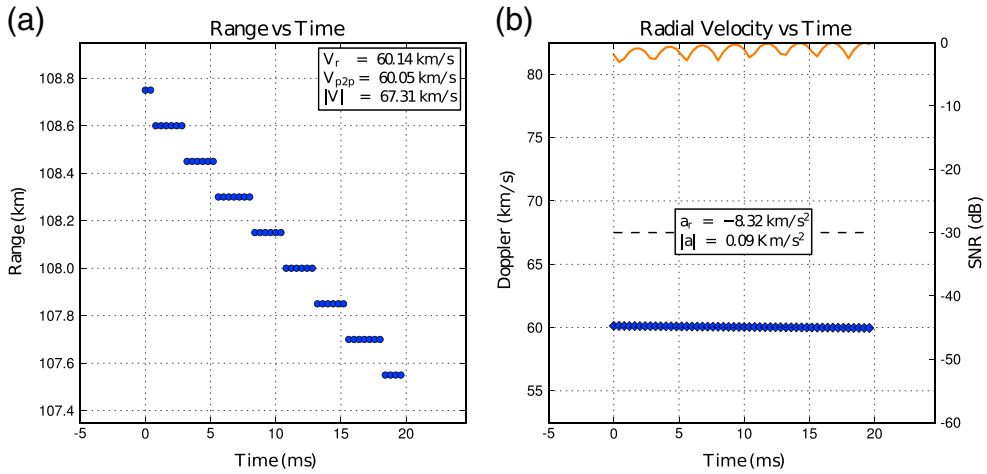

Figure 7. Similar to Figure 6, but showing an event with ~60 km/s radial velocity.

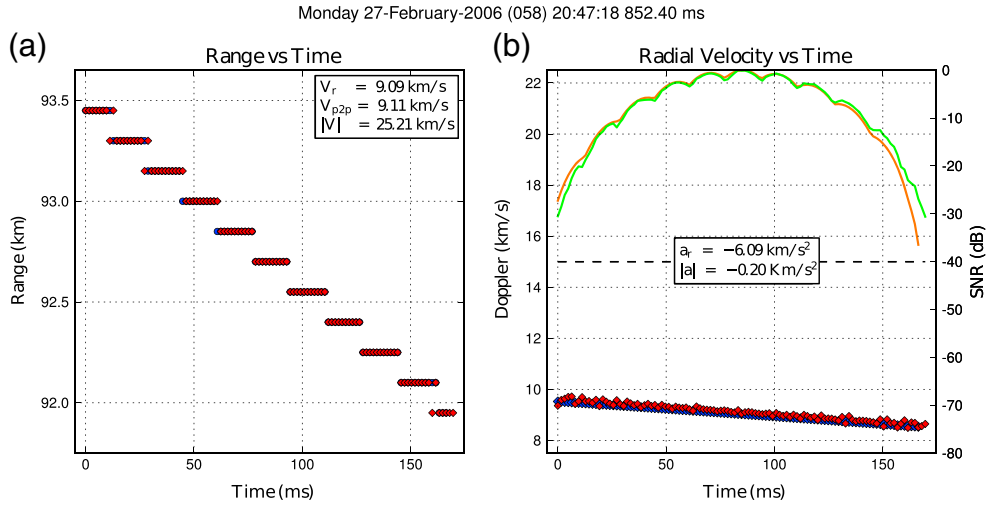

Figure 8. Simultaneous meteor comparison of experimental and simulated data for example presented in Figure 4.

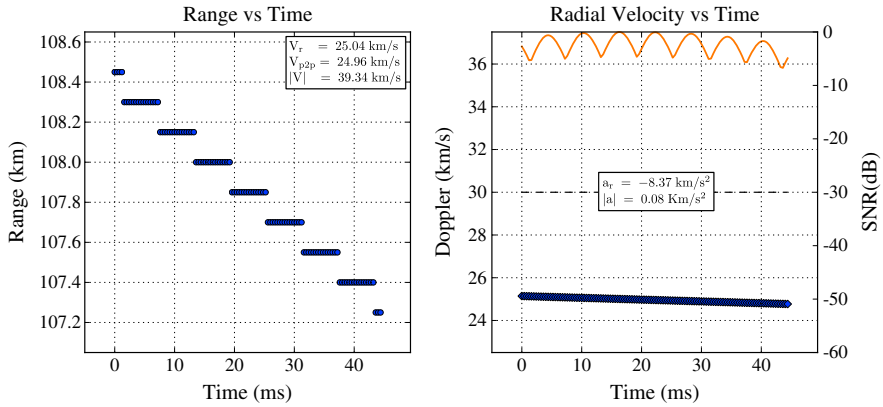

Figure 9. Similar to Figure 6, but using a different configuration of filters. We can see that the SNR values exhibit larger ripples.

the sampling parameters, and the signal processing used during the observation must be known. Herein, we discuss different parameters that affect the shape of the ripples produced in meteor SNR values.

1. The first parameter is the receiver filter. Equation (7) shows the relationship between the ripples in SNR and the receiver filter of radar systems. This relation is important because a different configuration of filters might result in larger ripples and therefore produce larger errors in meteor parameters obtained from SNR. For example, the same meteor can produce different SNR ripples when different combinations of filter are used. This clear contrast can be see in Figures 9 and 6.
2. The second parameter is the interpulse period. In sections 2.2 and 3.1 we explained the origin of the ripples in SNR as a result of changes in range of the meteor head echo from one IPP to the next one. Therefore the discrimination of ripples on meteor actual data will be a function of the IPP value. For example, if IPP = 2 ms and the Doppler velocity is 62.5 km/s, then the number of IPPs required for the meteor to travel through 150 m will be ~1 IPP because the meteor is changing its range in 125 m for IPP. In this case, the effective sampling will not produce enough samples to distinguish the ripple.
3. The third parameter is effective sampling. The effective sampling plays a role similar to the IPP value. For example, if IPP = 2 ms and the Doppler velocity is 62.5 km/s, then the number of IPPs required to travel through 600 m will be ~4. Equivalently, the meteor head echo will need more IPPs to travel through a longer resolution.
4. The fourth parameter is the pulse envelope. Figure 3 presented the ambiguity function for a pulse of length equal to 1 μ s and showed that the response in time is always wider than the radar range resolution, but they are still comparable. Thus we will observe temporal ripples in the SNR because of sampling different part of $|\chi(\tau,v_r)|$. In the case of a long noncoded pulse, the response in time will be much wider than the range resolution and therefore no fluctuations will be observed for samples in the flat region of the response. Figures 10a and 10b show these results. We used a long noncoded pulse of 10 μs, IPP = 0.4 ms

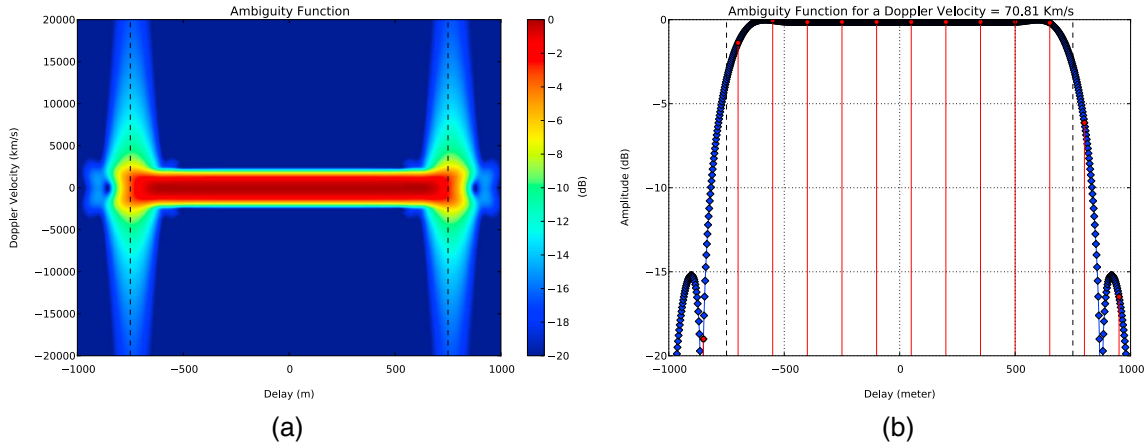

Figure 10. (a) Ambiguity function for a meteor observation at Jicamarca using a pulse with length T = $10\mu s$ and sampling rate of ts = $1\mu s$. (b) A cut of the ambiguity function for a Doppler velocity ~71 km/s. The red lines represent the actual data obtained after the decimation. The dashed lines in both plots represent the pulse width.

and effective sampling rate of 1 μs (red circles). If we average the expected SNR from this long noncoded pulse the temporal ripples would be smaller than the case presented in Figure 3. Notice that the sampling only plays an important role in the edges of $|\chi(\tau,v_r)|$.

5. The fifth parameter is the ensemble average. The ensemble average reduces the number of samples by a factor defined during the signal processing. At Jicamarca, meteor observations typically use 4 IPPs of 0.4 ms. As a result of this average, the ripplesmight get distorted if the number of final samples is not enough to define the shape of the ripples after the average. For example, if IPP = 0.4 ms and the Doppler velocity 62.5 km/s, then the number of IPPs required to travel through 150 m will be ~6 without averaging. Considering an average of 4 IPPs, the number of samples to define the ripples is reduced to ~1.5. Therefore the SNR should not show the features presented in Figures 4–7, and 8. Figure 11 shows an example from 5 May2007, where an ensemble average of 4 IPPs was applied.

6. Conclusions

[24] We reported the role that the ambiguity function plays in the determination of meteor SNR. This role was presented by expressing the radar equation for meteor head echoes in terms of the ambiguity function between the transmitted pulse envelope and filter impulse response of the receiver. The radar equation for meteor head echoes proves that the position of the meteor within the range cell affects the backscatter power estimate, and as a result of this process, any meteor SNR measured with any radar system will exhibit ripples. These amplitudes are related to the radar configuration that are been used. We should note that equation (7) was derived for constant Doppler velocity, but the same interpretation can be used in meteor events showing radial deceleration.

[25] This work is also supported with experimental data obtained using the 50 MHz radar from Jicamarca and simulated data obtained with a simulator of the radar receiver of Jicamarca. We showed that at least 14% of the

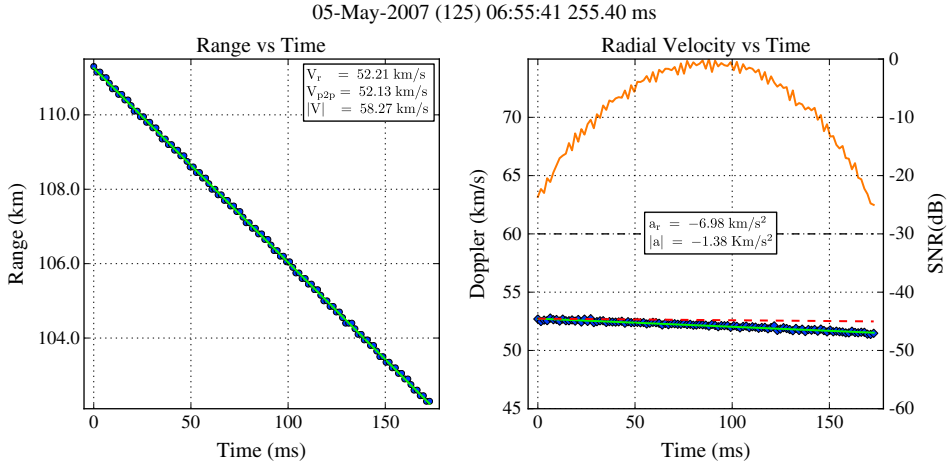

Figure 11. Effect of ensemble average in the actual meteor data

total population collected each day at Jicamarca present the ripples. Thus any approach (e.g., inversion techniques) to infer meteor head information correctly should only be applied to these events. On the remaining 86% of meteors, other sources of backscatter dominate the SNR measured and therefore the ripples can not be clearly distinguished.

[26] From section 5, we see that a quick strategy to mitigate the ripples is to work with a radar pulse width longer than the effective sampling, i.e., oversampling. Recently, *Kero et al*. [2012] introduced a technique to remove these ripples, which were detected using the Middle and Atmosphere radar, in Shigaraki, Japan. Our study showed the necessity of characterizing current radar systems for meteor head studies in order to infer unbiased meteor parameters correctly.

[27] **Acknowledgments.** The authors would like to thank the JRO (and IGP) staff for performing the observations, particularly to K. Kuyeng for her help in understanding the receiver system and A. Mills and R. Sorbello for helping us in the preparation of this manuscript.This work is supported by the National Science Foundation under grants ATM-0638624 and ATM-0457156 to Penn State University. The Jicamarca Radio Observatory is a facility of the Instituto Geofisico del Peru operated with support from the NSF AGS0905448through Cornell University.

References

Chau, J. L., and F. R. Galindo (2008), First definitive observations of meteor shower particles using high-power large-aperture radar, *Icarus*, *4*, 511–521.

Chau, J. L., and R. F. Woodman (2004), Observations of meteor head echoes using the Jicamarca 50 MHz radar in interferometer mode, *Atmos. Chem. Phys.*, *4*, 511–521.

Chau, J. L., R. F. Woodman, and F. R. Galindo (2007), Sporadic meteor sources as observed by the Jicamarca high-power large-aperture VHF radar, *Icarus*, *188*, 162–174.

Chau, J. L., F. R. Galindo, C. J. Heinselman, and M. J. Nicolls (2009), meteor head echo observations using an antenna compression approach with the 450 MHz Poker Flat Incoherent Scatter Radar, *J. Atmos. Sol. Terr. Phys.*, *71*, 636–643.

Close, S., M. Oppenheim, S. Hunt, and L. Dyrud (2002), Scattering characteristics of high-resolution meteor head echoes detected at multiple frequencies, *J. Geophys. Res.*, *107*(A10), 1295, doi:10.1029/2002JA009253.

Close, S., M. Oppenheim, S. Hunt, and A. Coster (2004), A technique for calculating meteor plasma density and meteoroid mass from radar head echo scattering, *Icarus*, *168*, 43–52.

Janches, D., L. P. Dyrud, S. L. Broadley, and J. M. C. Plane (2009), First observation of micrometeoroid differential ablation in the atmosphere, *Geophys. Res. Lett.*, *36*, L06101, doi:10.1029/2009GL037389.

Kero, J., C. Szasz, T. Nakamura, T. Terasawa, H. Miyamoto, and K. Nishimura (2012), A meteor head echo analysis algorithm for the lower VHF band, *Ann. Geophys.*, *30*, 639–659.

Kudeki, E. (2006), ECE 458 Lecture notes on applications of radiowave propagation, Dept. of Electr. and Comput. Eng., Univ. of Illinois at Urbana-Champaign.

Levanon, N. (1988), Radar Principles, Wiley, Hoboken, N. J.

Mathews, J. D., S. J. Briczinski, A. Malhotra, and J. Cross (2010), Extensive meteoroid fragmentation in V/UHF radar meteor observations at Arecibo Observatory, *Geophys. Res. Lett.*, *37*, L04103, doi:10.1029/2009GL041967.

Milla, M., and E. Kudeki (2006), F-region electron density and Te/Ti measurements using incoherent scatter power data collected at ALTAIR, *Ann Geophys.*, *24*, 1333–1342.

Nyquist, H. (1928), Thermal agitation of electric charge in conduction, *Phys. Rev.*, *32*, 110–113.

Ochs, G. (1965), The large 50 MC/S dipole array at Jicamarca radar observatory, report, Natl. Bur. of Stand., Gaithersburg, Md.

Roy, A., S. J. Briczinski, J. F. Doherty, and J. D. Mathews (2009), Genetic-algorithm-based parameter estimation technique for fragmenting radar meteor head echoes, *IEEE Geosci. Remote Sens. Lett.*, *6*(3), 363–367.

Siebert W. M. (1956), A radar detection philosophy, *IRE Trans. Inform. Theory*, *IT-2*, 204–221.

Texas Instruments (2001), GC 4016 Multi-standard quad DDC chip Data Sheet Rev 1.0, Dallas, Tex.

Vertatschitsch, L. E., J. D. Sahr, P. Colestock, and S. Close (2011), Meteoroid head echo polarization features studied by numerical electromagnetics modeling, *Radio Sci.*, *46*, RS6016, doi:10.1029/2011RS004774.

Woodman R. F. (1991), A general statistical instrument theory of atmospheric and ionospheric radars, *J. Geophys. Res.*, *96*(A45), 7911–7928.